

INTERACTION OF THE AGULHAS RINGS WITH TOPOGRAPHY IN REALISTIC SIMULATION

Maria Isabel dos Santos Barros
M1 Marine Physics - IUEM

Advisors:
Steven HERBETTE, UBO-IUEM/LOPS
Gildas CAMBON, (IRD, Brest)

June 26, 2020

Acknowledgements

I would like to thank my supervisor, Steven Herbette, for his guidance during this internship and disposition to help me understand the subject. Also, to Gildas Cambon, for helping with the many routines and for reading and correcting this report. To Wilton Aguiar, my friend and fellow oceanographer, for the never ending support, helping with the figures and listening to my troubles.

Contents

1	Introduction	2
1.1	Agulhas rings: formation and importance	2
1.2	Agulhas rings path and interaction with the bottom topography	3
1.2.1	Objective	4
1.2.2	Outline of the report	5
2	Materials & Methods	6
2.1	CROCO ocean model	6
2.2	Ability of the model to produce Agulhas rings	6
2.3	Eddy detection and tracking	7
2.3.1	Sea-surface height and surface geostrophic contours	7
2.3.2	The vorticity	7
2.3.3	Okubo-Weiss parameter	9
2.3.4	Eddy detection algorithm	9
2.3.5	Eddy tracking algorithm	9
2.4	Application to the detection of Agulhas rings and sensitivity test	10
3	Results	11
3.1	Tracking of eddies in the region	11
3.2	Case study: interaction of an eddy with the Agulhas ridge	11
3.2.1	Splitting of eddy 7774: consequences on the eddy characteristics . .	12
3.2.2	Blocking of eddy 8128 southward of the Agulhas ridge: consequences	13
3.3	Discussion and Conclusions	13
4	Annex	21
4.1	Materials and methods	21
4.1.1	Study region bathymetry	21
4.1.2	Sensitivity analysis	21

Chapter 1

Introduction

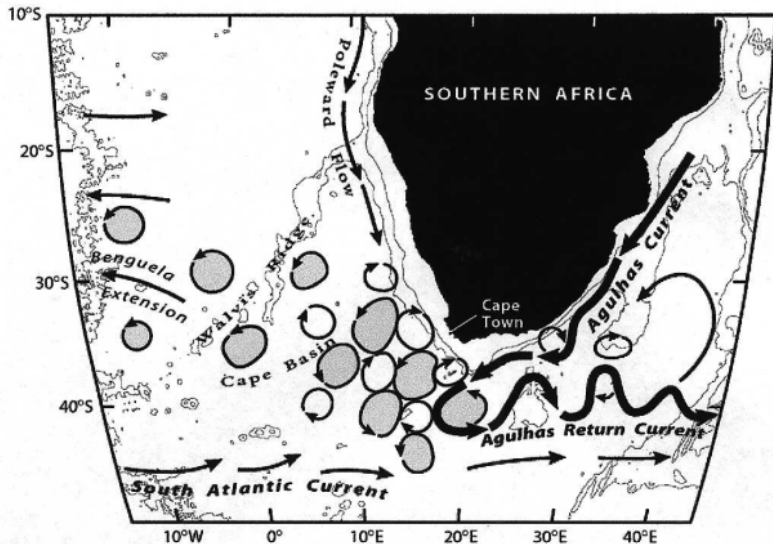


Figure 1.1: Schematic diagram of the Agulhas System Current System, the Agulhas Retroflection and the Agulhas rings. [After Boebel *et al.* (2003)]

1.1 Agulhas rings: formation and importance

Rings are intense-long-lived eddies that trap and transport waters that have the physical, chemical, and biological properties of their formation region (*Olson*, 1991). They can travel long distances, up to thousands of kilometers, and last from weeks to months. This expression was used for the first time by *Fuglister* (1972) when considering Gulf Stream rings formed from the looping of large meanders, closing onto themselves and subsequently detaching from the main current. Rings common formation areas are the western boundary currents, such as Kuroshio Current, Agulhas Current and the Gulf Stream.

The Agulhas rings are formed in the Agulhas Current System. The Agulhas Current is the western boundary current of the Indian Ocean subtropical gyre. It flows along the southeastern African shelf break (Fig. 1.1). When it reaches the southern tip of the African continent, it retroflects, veering backwards towards the Indian Ocean, and forms the Agulhas Return Current. Using thermal images to study the Retroflection's extension and variability, *Lutjeharms and Van Ballegooyen* (1988) conclude that the position of the

Agulhas retroflection varies from 16°E to 20°E.

The water masses transported within the Agulhas rings have similar characteristics to Indian Ocean waters. According to *Garzoli et al.* (1999) Agulhas rings are surface intensified eddies, their core being saltier, warmer and with less oxygen than their background. *Schmid et al.* (2003), in a autumn cruise of the KAPEX program in 1997, described the vertical structure of a young Agulhas Ring thanks to a cross section of temperature and salinity data. They found Indian Ocean Intermediate Water, Antarctic Intermediate Water, and waters from the Subtropical Front. Analyzing temperature salinity collected by Argo floats caught in a ring, *Guerra et al.* (2018) found similar results, identifying the South Indian Subtropical Mode Water and Subantarctic Mode Water.

The Agulhas rings play a major role in carrying warm and salty Indian Ocean waters into the Atlantic Ocean (*Olson and Evans*, 1986). This volume, heat and salt transport feed the upper branch of the Atlantic Meridional Overturning Circulation through the warm water route (*Beal et al.*, 2011). The Agulhas leakage occurs predominantly via rings, at the rate of 5-6/year (*Lutjeharms*, 1981; *Schouten et al.*, 2000; *Souza et al.*, 2011). Various estimates were made of their volume, heat and salt transport along the years. Estimates of volume transport by the Agulhas rings vary from 3 to 5 Sv (*Garzoli et al.*, 1999). *Byrne et al.* (1995) even estimated this volume transport to be of the order of 6.3–7 Sv. The heat transport varies between 0.027 calculated by *Souza et al.* (2011) and 0.47 PW/year calculated by *van Ballegooyen et al.* (1994). The salt transport were estimated as $0.42 \cdot 10^6$ kg/s by *van Ballegooyen et al.* (1994) and $0.13 \cdot 10^6$ kg/s by *van Aken et al.* (2003).

1.2 Agulhas rings path and interaction with the bottom topography

After they are being shed, the Agulhas rings leave the Retroflection and move northwestward into the Atlantic Ocean (Fig. 1.2) through the Cape Basin. *Dencausse et al.* (2010) suggested three main paths taken by the Agulhas rings to enter the South Atlantic Ocean: i) the northern route going along the African shelf; ii) the central route going roughly in the middle between African west coast and the Erica Seamount located on the eastern tip of the Agulhas Ridge; iii) the southern route going further east in the vicinity of the Agulhas ridge. When they reach the Cape Basin, Agulhas rings propagate northwestward, either advected by the Benguela Current and/or thanks to a self-advection mechanism.

Garzoli and Gordon (1996) described the Agulhas rings corridor (Fig.1.3). The corridor starts approximately at 37.5°S, 12.5°E and goes from 37°S, 20°E to 28°S, 0°, until the Walvis Ridge. Agulhas rings move at a mean speed of 5km/day and are influenced by their interaction with bottom topography (*Byrne et al.*, 1995; *Schouten et al.*, 2000).

Analysing the water mass properties of three Agulhas rings (R1, R2 and R3) surveyed in 1997 and reconstructing their path using altimetry data, *Ahran et al.* (1999) showed that Agulhas rings could evolve very differently according to their trajectory, and interaction with the topography. R1 had a colder (11°C) and more vertically homogenized core than the two other rings. It was shed by the Agulhas Retroflection in March 1994, and then spent the winter south of the Agulhas Ridge, hence suffering intense heat loss to the

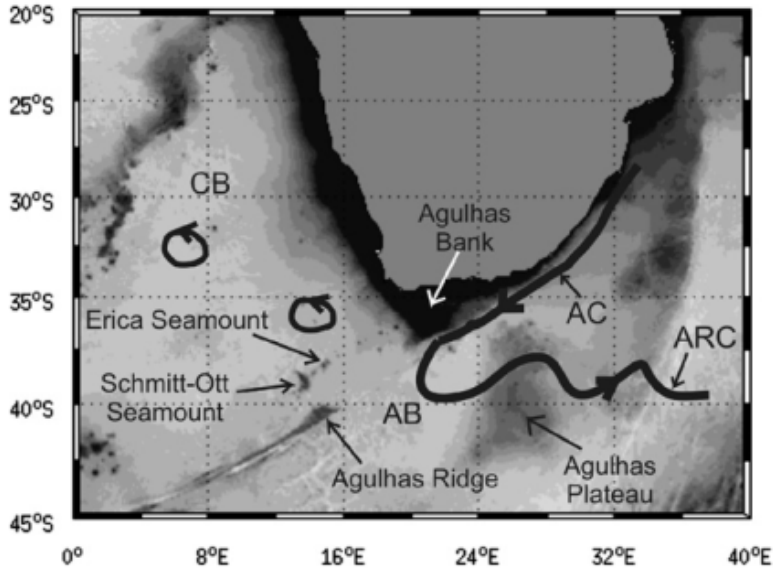


Figure 1.2: Bathymetry of the South-East Atlantic corner, highlighting the retroflexion of the Agulhas current, the shedding of rings and their subsequent northwestward path into the Cape basin through the Agulhas rings’ corridor. [After Dencausse *et al.* (2010)]

atmosphere.

R2 and R3 resulted from the splitting of one sole Agulhas ring. The splitting occurred when the latter encountered some isolated seamounts on the eastern flanks of the Agulhas ridge. Nevertheless, the two eddies were observed at different depth and with different water mass properties. R2 had a bigger radius and a warmer core made of 17.1°C Indian Ocean waters. Prior to its survey, it had followed a northwestward trajectory that brought it to warmer latitudes quickly after its formation. Despite resulting from the same eddy as R2, R3 had a colder ($\sim 13^{\circ}\text{C}$) and deeper core. Ahram *et al.* (1999) showed that it had remained blocked southward of the Agulhas ridge during the entire winter prior to its observation. Nevertheless, because the data comes from a single cruise, there was not enough lateral and temporal resolution to investigate the evolution of their vertical structure and the mixing of waters.

1.2.1 Objective

The main objective of this internship is to draw some statistics on the generation of Agulhas rings in a 3 km resolution simulation of the region, and infer some knowledge of their path, and potential interactions with the topography. In particular, we focus on an Agulhas ring that resulted from the splitting of a large one after encountering the Erica seamount, and that remained blocked south of the Agulhas Ridge.

In this internship we use a simulation from the Regional Ocean Model System (ROMS) in its CROCO version for investigating the vertical structure evolution of two eddies using temperature and salinity cross sections.

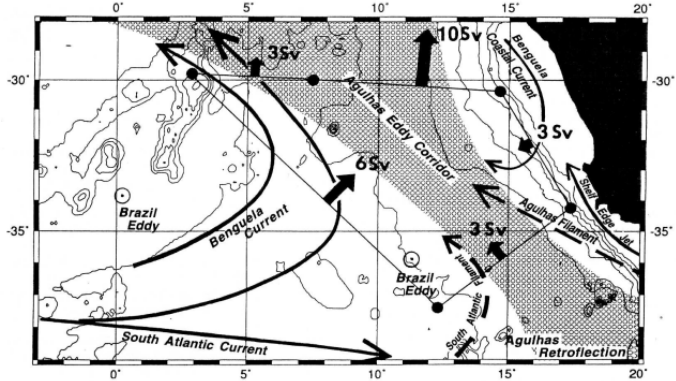


Figure 1.3: Schematic diagram of the Agulhas rings corridor and their transport in the South Atlantic Ocean [After Garzoli and Gordon (1996)]

1.2.2 Outline of the report

Section 2 describes the model simulation as well as some key fundamental theoretical quantities used to characterize eddies. The algorithm used to identify and track eddies is presented in details, as its implementation constituted a significant part of my work. In section 3, we give a census of anticyclonic eddies that interacted with the Agulhas ridge, and focus on the evolution of one eddy that split as it interacted with the Agulhas ridge. Finally, a discussion with some concluding remarks and perspectives are presented section 4.

Chapter 2

Materials & Methods

In this chapter the model configuration will be presented, followed by the theoretic basis for eddies characterization and finally, we present the eddy detection and tracking method.

2.1 CROCO ocean model

The Coastal and Regional Ocean Community Model is based on Regional Ocean Modeling System with online grid nesting capabilities (AGRIF) (*Debreu et al.*, 2012; *Shchepetkine and McWilliams*, 2005), and maintained by several French institutes, IRD, INRIA, CNRS, IFREMER and SHOM. CROCO is an ocean circulation model that resolves the primitive equations, which are simplifications of the Navier-Stokes equations. The horizontal discretization is in orthogonal-curvilinear coordinate system and the variables are computed in an Arakawa C-grid, where the velocity is at the corners and SSH, vorticity, and ρ are computed at the center of the grid (*Arakawa and Lamb*, 1977). The vertical discretization is in σ following-coordinates that follow the terrain.

The model grid extends from 8° - 28° E and 44° - 24° with a horizontal resolution of 3 km, and 75 vertical sigma levels (BENGR3KM configuration). The model was run from 1990 to 2011 with daily outputs. It was forced at the lateral boundaries by coarser CROCO outputs originating from a 7km resolution simulation. At the surface atmospheric boundaries, the model was forced by 6-hourly CFSR forcing (Fig 2.1). A detailed description of the BENGR3KM configuration is detailed in (*Ragoasha*, 2020). In this study, we used a geographical subset of the BENGR3KM configuration, presented on the Fig. 2.1.

2.2 Ability of the model to produce Agulhas rings

The model can reproduce the shedding of Agulhas rings and their subsequent advection towards the South Atlantic. As an illustration, we show a series of surface vorticity maps (Fig. 2.2). The Agulhas Current first forms a large meander south, creating a large loop. When the loop closes onto it self, it forms a large anticyclonic eddy that detaches from the main current propagating westward.

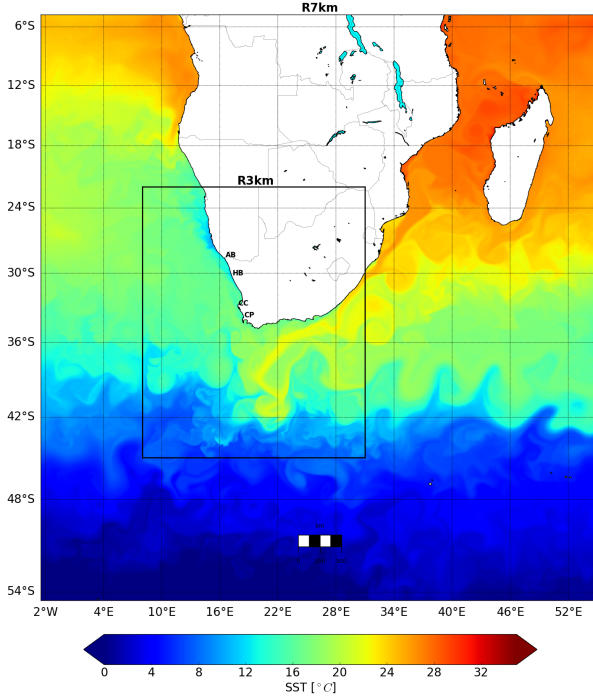


Figure 2.1: Snapshot of SST (Year 2005, 1st of January). The black box delineates the boundaries of the nested 3 km child grid. Within the box, the SST of the 3 km simulation is superimposed upon the one of the 7 km simulation. Figure from *Ragoasha (2020)*

2.3 Eddy detection and tracking

We are interested in spotting Agulhas rings that will interact with the Agulhas ridge. Our first task has been to detect and track the eddies that interacted with ridge.

2.3.1 Sea-surface height and surface geostrophic contours

Geostrophic flow may be used to study the dynamics of mesoscale eddies provided their Rossby number remains low enough. For this internship, we will study the dynamic characteristics of the Agulhas eddies using the superficial vorticity and the Okubo-Weiss parameter. The geostrophic velocities are first calculated from the Sea Surface Height, η , as follows:

$$u_g = -\frac{g}{f} \frac{\partial \eta}{\partial y} \quad (2.1)$$

$$v_g = \frac{g}{f} \frac{\partial \eta}{\partial x} \quad (2.2)$$

2.3.2 The vorticity

Relative vorticity ξ measures the rotation rate of fluid particles in the horizontal plane:

$$\xi_v = \frac{\partial v}{\partial x} - \frac{\partial u}{\partial y} \quad (2.3)$$

It can also be seen as the z-component of the curl of the 3D-velocity field

$$\xi = \nabla \times \vec{V}$$

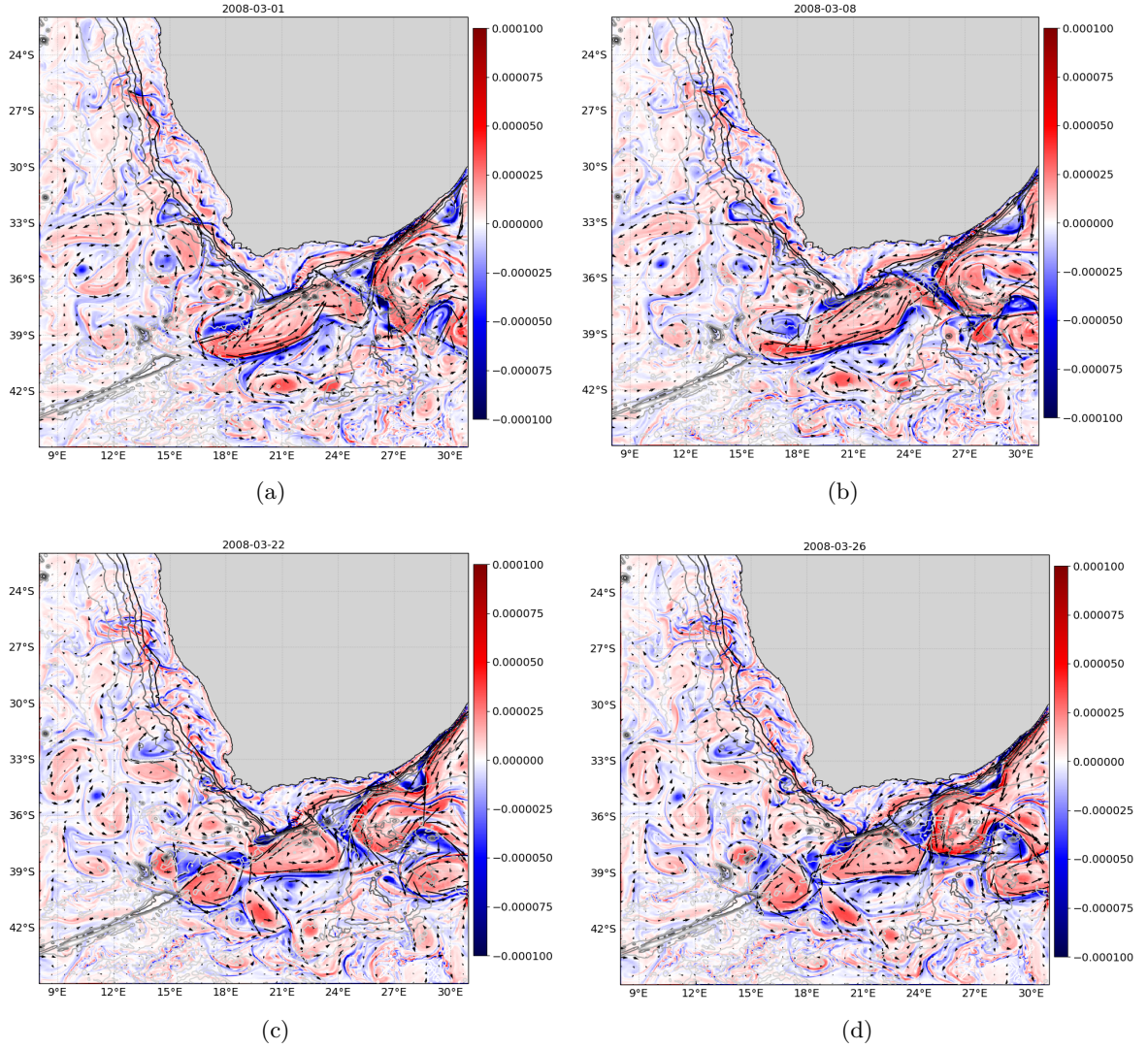


Figure 2.2: Surface vorticity map with the sequence of Agulhas meandering *a*), when the meandering is closing Ridge *b*), on the splitting process *c*) and after splitting an eddy is observed *d*)

2.3.3 Okubo-Weiss parameter

From u_g and v_g (Eqs. 2.1 - 2.2) we evaluate the deformation of the flow compared to the strain using the Okubo-Weiss parameter (*Okubo*, 1970; *Weiss*, 1991; *Isern-Fontanet et al.*, 2006). It is defined by:

$$W = S_n^2 + S_s^2 - \omega^2, \quad (2.4)$$

where S_n and S_s are the normal component and shear components of the strain, respectively:

$$S_n = \frac{\partial u}{\partial x} - \frac{\partial v}{\partial y} \quad (2.5)$$

$$S_s = \frac{\partial v}{\partial x} + \frac{\partial u}{\partial y} \quad (2.6)$$

and ω is the relative vorticity. We can find vortices where there is predominance of vorticity over strain, thus the areas of $W < 0$.

2.3.4 Eddy detection algorithm

The eddy detection algorithm is based on a combination of a geometric criteria that looks for closed contours of Sea Surface Height (SSH), and some constraints on dynamic properties of the flow through the Okubo-Weiss parameter W (*Chelton et al.*, 2007; *Halo et al.*, 2014). When $W < W_{threshold}$, vorticity dominates the strain, and one may consider that there is an eddy flow. This method can be described by the following steps:

1. Local maxima and minima of SSH are identified for each daily map.
2. A sub-domain of 300 km around each local extreme is created.
3. In case a local extreme is detected, the algorithm looks for the existence of adjacent closed iso-contours of SSH around this point. It selects the most outward closed contour after testing contours separated by a 2 cm interval.
Only eddies with more than 4 pixels are kept.
4. The Okubo-Weiss parameter is calculated from geostrophic velocities.
5. The regions of $W < W_{threshold}$ are selected inside the previously selected closed contours.

2.3.5 Eddy tracking algorithm

These steps are applied to the daily outputs of model SSH. The algorithm for eddy tracking compares two eddies identified on two consecutive days and considers them to be the same eddy if the generalized distance between them is minimum (*Penven et al.*, 2005; *Halo et al.*, 2014):

$$X_{e_1, e_2} = \sqrt{(\frac{L}{L0})^2 + (\frac{\delta R}{R0})^2 + (\frac{\delta X}{X0})^2 + (\frac{\delta Z}{Z0})^2 + (\frac{\delta A}{A0})^2} \quad (2.7)$$

where L_0 , R_0 X_0 , Z_0 and A_0 are typical eddy distance of 60 km, radius scale of 30 km, vorticity scale, 10^{-5} , Mean SSH of 10cm and amplitude. In order to be considered the same eddy, the speed calculated should also be compatible with a maximum value, 50 cm/s.

Two or more local extreme are often detected close to each other, which causes oversampling of the eddies. In order to prevent that, at each iteration on the eddy identification routine, we excluded all the local maxima and minima inside the area delimited by the outermost contour.

2.4 Application to the detection of Agulhas rings and sensitivity test

Sensitivity tests are performed in order to tune the parameters of the eddy detection algorithm and evaluate its capacity to detect Agulhas rings. In order to reduce noise in the Okubo-Weiss data, we utilize a Hanning filter. After passing the Hanning filter three times, there were no major improvements. Then, to ensure that the closed contours of SLA corresponded to mesoscale vortices, and avoid ocean gyres or smaller structures, the radius of the detected eddies is further limited: $30 \text{ km} < R_{\text{eddy}} < 300 \text{ km}$.

We tested 10 and 30 km values for the minimum threshold radius, 100 and 300 km for the maximum threshold radius. When choosing 100 km, we lose the largest mesoscale structures that are of interest for this study. Because we are interested in the bigger anticyclones and because there was no significant losses on the number of identified eddies, the minimum threshold of 30 km was chosen. Hence, the following parameters were chosen: the radius of the chosen eddies would be between 30 and 300 km, passing Hanning filter two times.

Chapter 3

Results

3.1 Tracking of eddies in the region

In this work 9680 different mesoscale eddies were identified and tracked from 2005 to 2008. In Fig. 3.1 we show the trajectories of anticyclones that were generated between 16° E and 20° E penetrating into the South Atlantic Ocean.

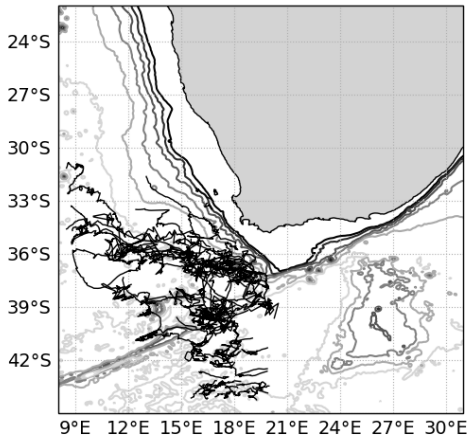


Figure 3.1: Anticyclones that got into the South Atlantic Ocean

We identified 17 eddies with mean radius size bigger than 30km that interacted with the Agulhas Ridge for at least 5 days. The characteristics of these 17 eddies are listed in table 3.1. Their mean radius size varied from 30 km to 96 km. The mean radius of these eddies was smaller than the ones that take the northern route, which was also observed by *Pilo et al.* (2015) in their census of the trajectories of eddies originating from the Agulhas Current for 1992 to 2012.

3.2 Case study: interaction of an eddy with the Agulhas ridge

From these eddies, two were particularly interesting. They are the ones labelled ID7774 and ID8128. The latter actually resulted from the splitting of the former. The splitting

ID	Vorticity [1/s]	Life time[days]	Season	Days near ridge	Radius[km^2]
15	1,84E-05	102	Summer	20	96.24
32	-2,06E-05	108	Summer	9	48.80
550	-9,54E-06	99	Autumn	10	45.62
1109	1,92E-05	134	Winter	21	106.71
1288	-2,33E-05	54	Winter	6	52.42
1758	1,15E-05	243	Summer	89	48.66
3506	2,41E-05	108	Winter	21	60.24
3818	-8,21E-06	148	Winter/Spring	44	48.94
3841	2,97E-05	36	Winter	10	46.266
4043	-4,11E-05	87	Spring	6	32.399
4312	2,46E-05	171	Spring	29	66.775
5962	1,00E-05	78	Winter	64	35.762
7471	-3,76E-05	132	Summer	23	43.668
7774	1,54E-05	254	Autumn	39	87.516
8128	1,87E-05	158	Autumn/Winter	40	53.975
8560	-3,43E-05	143	Winter	6	46.418
9302	2,66E-05	21	Spring	10	42.957

Table 3.1: Properties of eddies interacting with the Agulhas ridge

event is illustrated in Fig. 3.2. Eddy 7774 was first detected on March, 15th. Eddy 7774 started to interact with the eastern part of the ridge on March, 26th. It stayed close to the ridge for 39 days. On May, 5th it split into two eddies and eddy 8128 was first spotted. Finally the eddy 7774 moved northward towards the Cape Basin, following a northwestward trajectory. Contrary to 7774 that quickly propagated towards lower latitudes, eddy 8128 stayed most of winter blocked behind the Agulhas ridge. Hence, this eddy is expected to have experienced strong winter cooling, which may have caused some changes in its vertical hydrographic structure.

3.2.1 Splitting of eddy 7774: consequences on the eddy characteristics

In order to assess the consequences of the splitting on the vertical structure of the eddy, we choose to perform vertical transects across the two eddies, before the splitting and two weeks after the splitting. The first section is performed through eddy 7774, on May 4th, just when the eddy passes the Agulhas ridge after remaining blocked southward of it for a month (Fig. 3.3). The second section occurs on May 24th, after the splitting occurred: the remaining part of eddy 7774 has moved northward, where as eddy 8128 has remained southward of the Agulhas ridge (Fig. 3.4).

Before the splitting, the characteristics of eddy 7774 are typical of an Agulhas ring. It is a large (radius \simeq 90 km) surface intensified eddy with a strong signature in sea surface height (SSH \simeq 0.39 m). It is made of an anticyclonic lens that extends as deep as 1500 m. The eddy core is located in the upper 1000 m, and constituted of warm ($18^\circ C$) and salty (35.5 PSU) waters (Fig. 3.3). After the splitting, eddy 7774 has a smaller radius (\simeq 75 km) but the amplitude in SLA remains similar (\simeq 0.39 m), the $10^\circ C$ isotherm moved upward from 660 to 560m.

After the splitting, eddy 7774 lost volume but continued to have a strong signature in

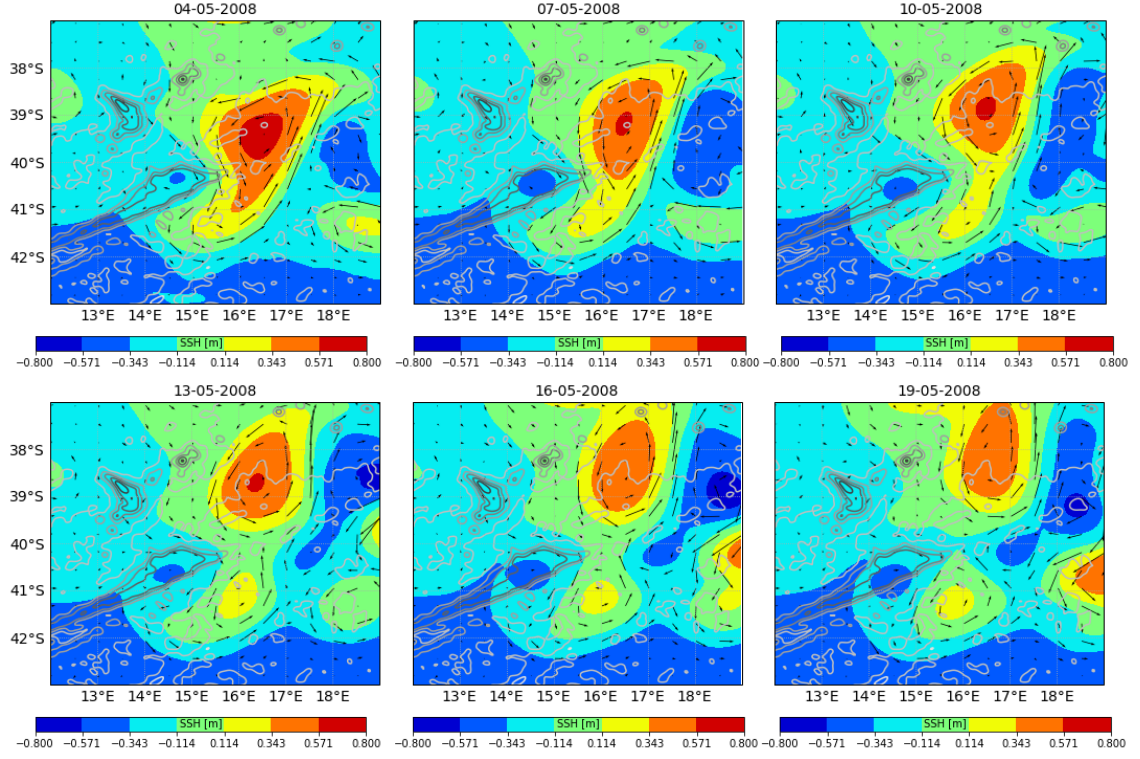


Figure 3.2: Snapshots of Sea Surface Height and surface currents during the splitting of eddy 7774

SSH, and a similar vertical structure. Eddy 8128 was much smaller (radius \approx 50 km), and more surface intensified (Fig. 3.4). Hence, the splitting probably mainly took place in the upper layers of the eddy.

3.2.2 Blocking of eddy 8128 southward of the Agulhas ridge: consequences

A month after the splitting event, the two resulting eddies have evolved very differently. On 24th, June 2008, eddy 8128 has just spent more than a month blocked southward of the ridge at high latitudes, whereas eddy 7774 has propagated northward into the Cape basin and is now located at 36°S (Fig. 3.5). Across-eddy vertical transects through both eddies show very different structure. While eddy 8128 was a month earlier more stratified and upper intensified than eddy 7774 (Fig. 3.5), it now appears to be much colder than eddy 7774. The surface temperature difference is around 1.5° C and this difference increases with depth, up to 4° at 400m. Additionally, eddy 7774 is more stratified, while eddy 8128 have a more homogeneous vertical structure (fig. 3.5).

3.3 Discussion and Conclusions

These results have shown that the model was able to reproduce the interaction of Agulhas rings with the Agulhas ridge. This interaction can lead to the splitting of the eddies and slow down their northwestward advection into the South Atlantic. *Dencausse et al.* (2010) analyzed the trajectories of 199 Agulhas rings from 1992 to 2007 and found that 46% of

04-05-2008

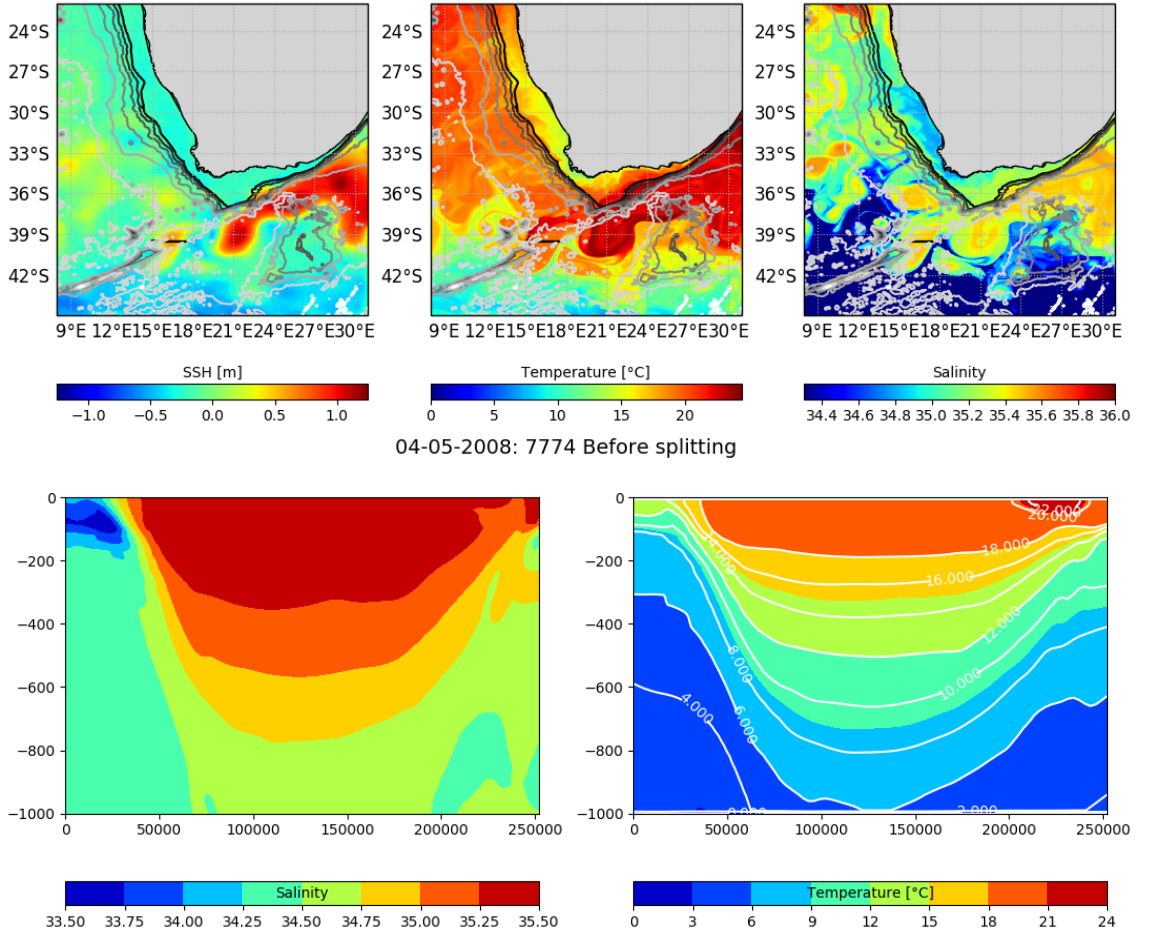


Figure 3.3: Maps of SSH, temperature and salinity (top) and temperature/salinity vertical sections across eddy 7774 (bottom) on 4th, May, 2008. At that time, the eddy 7774 started to interact with the Agulhas Ridge. The black line on the top sub-figure indicates the location of the across-eddy transect.

24-05-2008

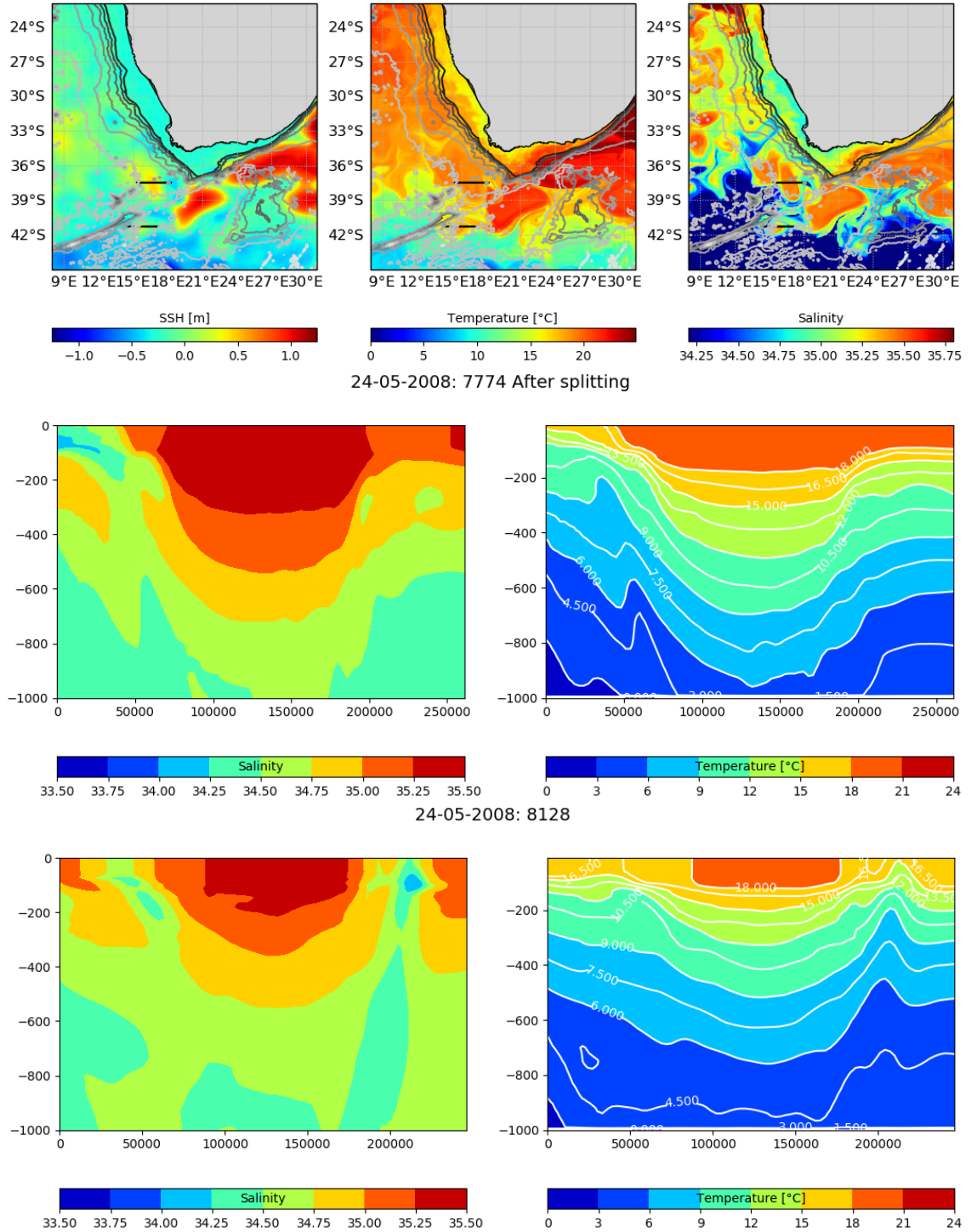


Figure 3.4: Maps of SSH, temperature and salinity (top) and temperature/salinity vertical sections across eddy 7774 (bottom) and eddy 8128 (bottom) on 24th, May, 2008. At that time, eddy 7774 had split into two eddies. The black lines on the top sub-figure indicates the location of the across-eddy transects.

24-06-2008

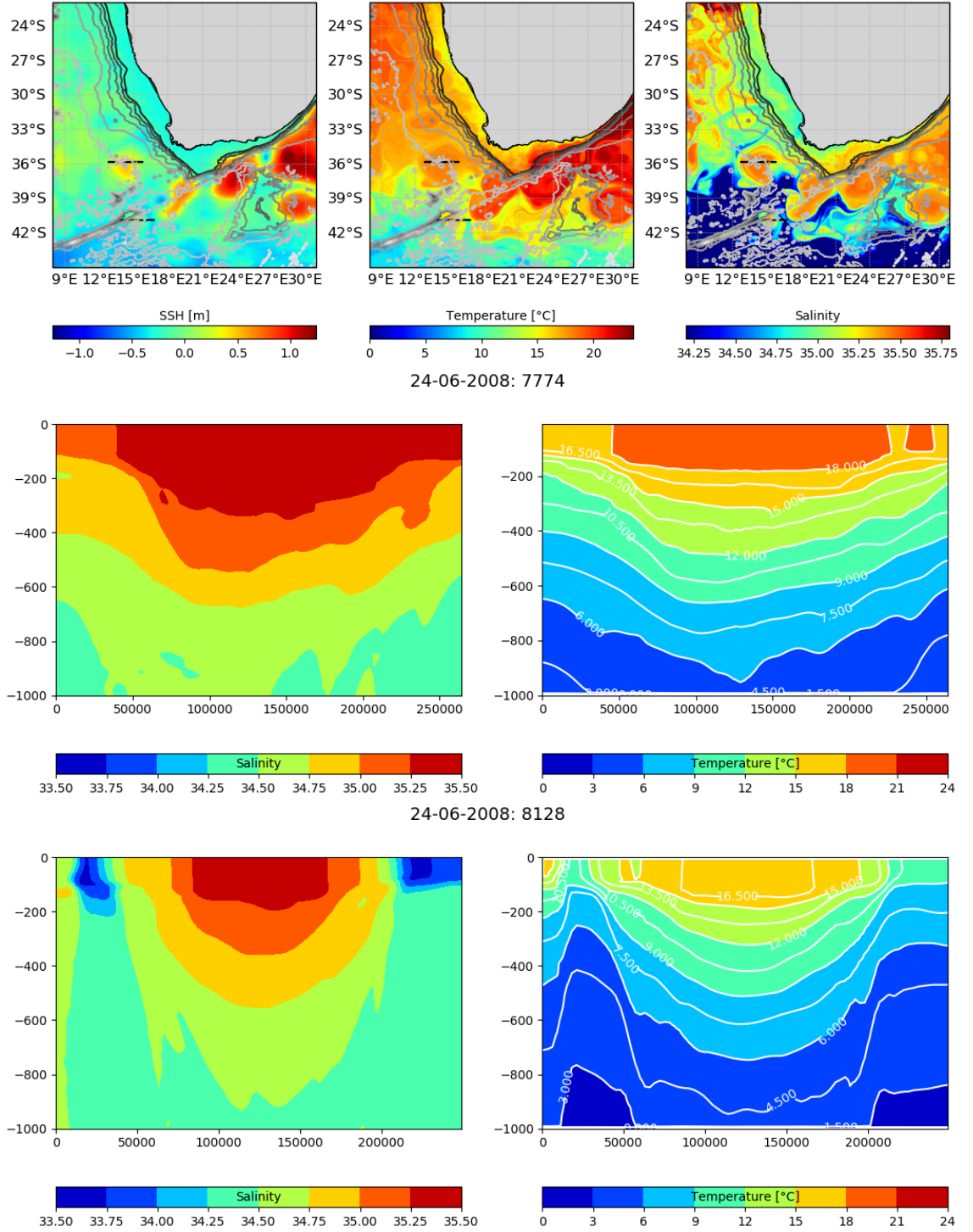


Figure 3.5: Maps of SSH, temperature and salinity (top) and temperature/salinity vertical sections across eddy 7774 (bottom) and eddy 8128 (bottom) on 24th, June, 2008. This time is 6 weeks after the splitting eddy 7774. The two eddies have evolved very differently. The black lines on the top sub-figure indicates the location of the across-eddy transects.

them suffered splitting. *Ahran et al.* (1999) also observed splitting events when Agulhas rings reach and interact with the Walvis Ridge, specially and the Vema Seamount. *Dencausse et al.* (2010) also found that in fifteen years a third of Agulhas rings took the southern route, interacting with the Agulhas ridge.

For the case studied here, the splitting mostly impacted the upper layers of the eddy. The upper part of an Agulhas ring was torn off to form a second, eddy that was smaller in size and amplitude.

The two eddies evolve very differently. Eddies that stay block behind the ridge experience cooling which modifies their vertical structure. Their core gets cooler and more homogenized. The eddies that propagate northwestward towards warmer waters become more stratified. There is a resemblance of this event with the rings observed by *Ahran et al.* (1999), R1 and R2. Similarly to eddy 8128, R1 stayed behind the Agulhas ridge all winter, lost heat to the atmosphere and had a colder core and more homogeneous structure. However, R1 suffered even more wintering, so its core is even colder and more homogeneous than 8128. R2, a bigger and more superficial ring, spent less time on higher latitudes and didn't suffer cooling, keeping Indian Water characteristics, as eddy 7774.

Agulhas rings carry salty and warm water from the Indian into the South Atlantic Ocean, having an important influence on the vertical structure (*Olson and Evans*, 1986). *Schouten et al.* (2000) indicate that a third of the rings dissipate on Cape Basin, exchanging heat and salt with the background, having an important input to the Atlantic thermohaline circulation (AMOC). *Dencausse et al.* (2010) found that rings that go through the central route, and thus between the Agulhas ridge and the Erica seamount, are responsible for half of the total volume transport. *Ahran et al.* (1999) also affirm that the Agulhas ridge has a key role on the warm water transport from the Indian Ocean.

In order to estimate correctly these fluxes, it is important that the models can reproduce properly the rings that go in this route, as well as the ones that stay behind the ridge. Important next steps would be: i) Differentiate the Agulhas rings from other anticyclones in order to assess the model capacity to reproduce them on the right numbers; ii) analyze the rings vertical structure evolution during all their life cycle so to investigate with more details the wintering effect and ii) calculate their heat and salt content.

Bibliography

- Ahran, M., H. Mercier, and J. R. E. Lutjeharms (1999), The disparate evolution of three agulhas rings in the south atlantic ocean, *Journal of Geophysical Research*, 104, 20,987–21,005, doi:10.1029/1998jc900047.
- Arakawa, A., and V. R. Lamb (1977), Computational design of the basic dynamical processes of the ucla general circulation model, *General circulation models of the atmosphere*, 17(Supplement C), 173–265.
- Beal, L. M., et al. (2011), On the role of the agulhas system in ocean circulation and climate, *Nature*, 472, 429–436, doi:10.1038/nature09983.
- Boebel, O., J. R. E. Lutjeharms, C. Schid, W. Zenk, T. Rossby, and Barron (2003), The cape cauldron: a regime of turbulent inter-ocean exchange, *Deep Sea Research Part II: Topical Studies in Oceanography*, 50(1), 57–86, doi:10.1016/S0967-0645(02)00379-X10.1175/2008JTECHO541.1.
- Byrne, D. A., A. L. Gordon, and W. F. Haxby (1995), Agulhas eddies: A synoptic view using geosat rm data, *Journal of Physical Oceanography*, 25(5), 902–917, doi:10.1016/j.pocean.2011.01.002.
- Chelton, D. B., M. G. Schlax, R. M. Samelson, and R. A. de Szoeke (2007), Global observations of large oceanic eddies, *Geophysical Research Letters*, 34(15).
- Debreu, L., P. Marchesiello, P. Penven, and G. Cambon (2012), Two-way nesting in split-explicit ocean models: Algorithms, implementation and validation, *Ocean Modelling*, 49-50, 1–21, doi:10.1016/j.ocemod.2012.03.003.
- Dencausse, G., M. Arhan, and S. Speich (2010), Routes of agulhas rings in the southeastern cape basin, *Deep Sea Research Part I: Oceanographic Research Papers*, 57(11), 1406–1421, doi:<https://doi.org/10.1016/j.dsr.2010.07.008>.
- Fuglister, F. C. (1972), Cyclonic rings formed by the gulf stream 1965-66, *Studies in Physical Oceanography: A Tribute to Georg Wust on His 80th Birthday*, pp. 137–168.
- Garzoli, S. L., and A. L. Gordon (1996), Origins and variability of the benguela current, *Journal of Geophysical Research: Oceans*, 101(C1), 897–906, doi:10.1029/95JC03221.
- Garzoli, S. L., P. L. Richardson, C. M. Duncombe Rae, D. M. Fratantoni, G. J. Goñi, and A. J. Roubicek (1999), Three agulhas rings observed during the benguela current experiment, *Journal of Geophysical Research: Oceans*, 104(C9), 20,971–20,985, doi:10.1029/1999JC900060.

- Guerra, L. A. A., A. M. Paiva, and E. P. Chassignet (2018), On the translation of agulhas rings to the western south atlantic ocean, *Deep Sea Research Part I: Oceanographic Research Papers*, 39, 104 – 113, doi:<https://doi.org/10.1016/j.dsr.2018.08.005>.
- Halo, I., B. Backeberg, P. Penven, I. Ansorge, C. Reason, and J. Ullgren (2014), Eddy properties in the mozambique channel: A comparison between observations and two numerical ocean circulation models, *Deep Sea Research Part II: Topical Studies in Oceanography*, 100, 38 – 53, doi:<https://doi.org/10.1016/j.dsr2.2013.10.015>, the Mozambique Channel: Mesoscale Dynamics and Ecosystem Responses.
- Isern-Fontanet, J., E. García-Ladona, and J. Font (2006), Vortices of the mediterranean sea: An altimetric perspective, *Journal of physical oceanography*, 36(1), 87–103.
- Lutjeharms, J. R. E. (1981), Features of southern agulhas current circulation from satellite remote sensing, *South African Journal of Science*, 77(5), 231–236.
- Lutjeharms, J. R. E., and R. C. Van Ballegooyen (1988), The Retroflection of the Agulhas Current, *Journal of Physical Oceanography*, 18(11), 1570–1583, doi:[10.1175/1520-0485\(1988\)018<1570:TROTAC>2.0.CO;2](https://doi.org/10.1175/1520-0485(1988)018<1570:TROTAC>2.0.CO;2).
- Okubo, A. (1970), Horizontal dispersion of floatable particles in the vicinity of velocity singularities such as convergences.
- Olson, D. B. (1991), Rings in the ocean, *Annual Review of Earth and Planetary Sciences*, 19(1), 283–311.
- Olson, D. B., and R. H. Evans (1986), Rings of the agulhas current, *Deep-Sea Research*.
- Penven, P., V. Echevin, J. Pasapera, F. Colas, and J. Tam (2005), Average circulation, seasonal cycle, and mesoscale dynamics of the peru current system: A modeling approach, *Journal of Geophysical Research: Oceans*, 110(C10).
- Pilo, G. S., M. M. Mata, and J. L. L. Azevedo (2015), Eddy surface properties and propagation at southern hemisphere western boundary current systems, *Ocean Science*, 11(4), 629–641, doi:[10.5194/os-11-629-2015](https://doi.org/10.5194/os-11-629-2015).
- Ragoasha, M. N. (2020), The variability of lagrangian transport in the southern benguela current upwelling system, Ph.D. thesis, University of Cape Town / University of Brest.
- Schmid, C., O. Boebel, W. Zenk, J. Lutjeharms, S. Garzoli, P. Richardson, and C. Barron (2003), Early evolution of an agulhas ring, *Deep Sea Research Part II: Topical Studies in Oceanography*, 50(1), 141 – 166, doi:[https://doi.org/10.1016/S0967-0645\(02\)00382-X](https://doi.org/10.1016/S0967-0645(02)00382-X), inter-ocean exchange around southern Africa.
- Schouten, M. W., W. P. M. de Ruijter, P. J. van Leeuwen, and J. R. E. Lutjeharms (2000), Translation, decay and splitting of agulhas rings in the southeastern atlantic ocean, *Journal of Geophysical Research: Oceans*, 105(C9), 21,913–21,925, doi:[10.1029/1999JC000046](https://doi.org/10.1029/1999JC000046).
- Shchepetkin, A. F., and J. C. McWilliams (2005), Regional Ocean Modeling System: A split-explicit ocean model with a free-surface and topography-following vertical coordinates., *Ocean Modelling*, 9, 347–404.

- Souza, J. M. A. C., C. de Boyer Montégut, C. Cabanes, and P. Klein (2011), Estimation of the agulhas ring impacts on meridional heat fluxes and transport using argo floats and satellite data, *Geophysical Research Letters*, 38(21), doi:10.1029/2011GL049359.
- van Aken, H., A. van Veldhoven, C. Veth, W. de Ruijter, P. van Leeuwen, S. Drijfhout, C. Whittle, and M. Rouault (2003), Observations of a young agulhas ring, astrid, during mare in march 2000, *Deep Sea Research Part II: Topical Studies in Oceanography*, 50(1), 167–195, doi:[https://doi.org/10.1016/S0967-0645\(02\)00383-1](https://doi.org/10.1016/S0967-0645(02)00383-1), inter-ocean exchange around southern Africa.
- van Ballegooyen, R. C., M. L. Gründlingh, and J. R. E. Lutjeharms (1994), Eddy fluxes of heat and salt from the southwest indian ocean into the southeast atlantic ocean: A case study, *Journal of Geophysical Research: Oceans*, 99(C7), 14,053–14,070, doi: 10.1029/94JC00383.
- Weiss, J. (1991), The dynamics of enstrophy transfer in two-dimensional hydrodynamics, *Physica D: Nonlinear Phenomena*, 48(2-3), 273–294.

Chapter 4

Annex

4.1 Materials and methods

4.1.1 Study region bathymetry

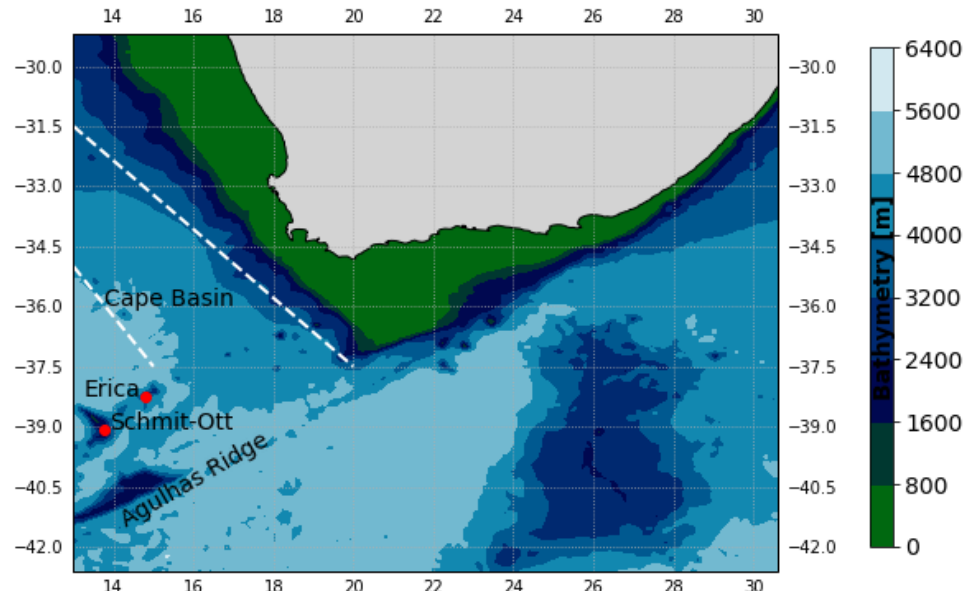


Figure 4.1: Main features of the study region. In white, the Agulhas rings corridor based on *Garzoli and Gordon (1996)*

4.1.2 Sensitivity analysis

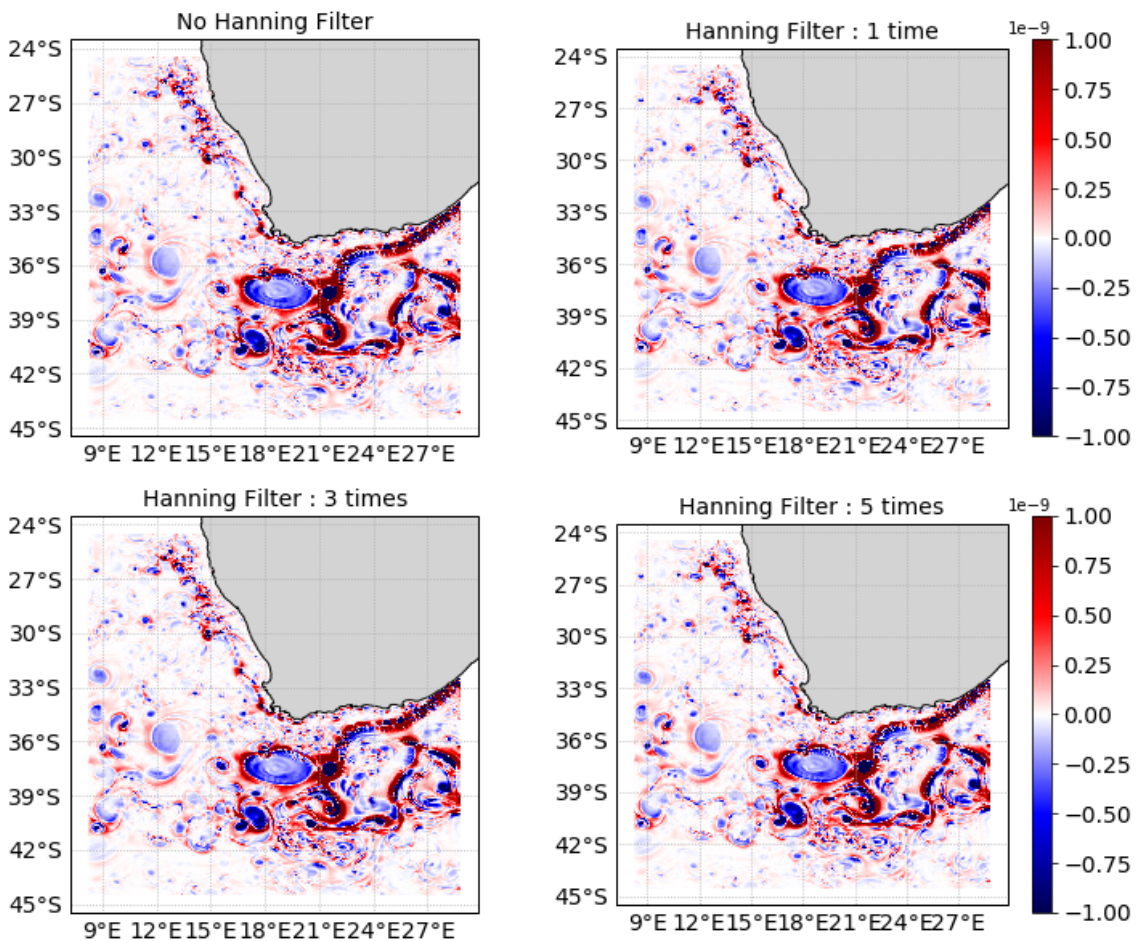


Figure 4.2: The Okubo Weiss parameter with: a) No filter, b)one time, c)three times and d)five passes of Hanning Filter

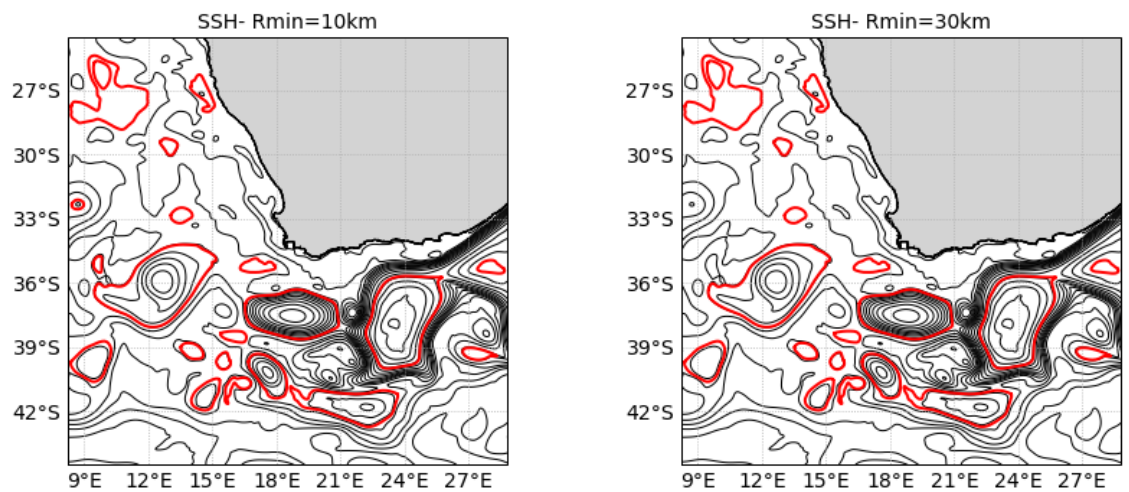


Figure 4.3: Evaluation of the detection of eddies for minimum radius of 10km and 30km, respectively

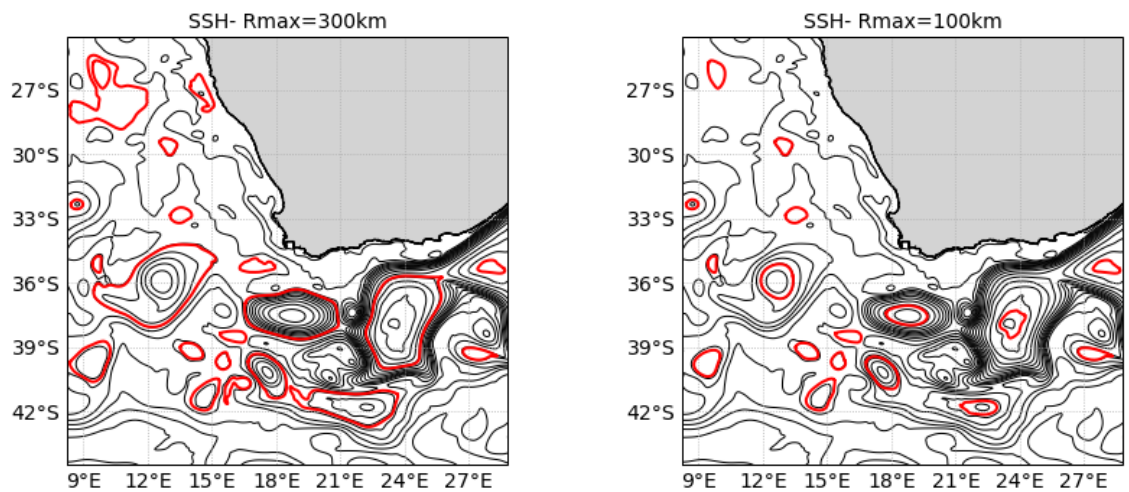


Figure 4.4: Evaluation of the detection of eddies for maximum radius of 100km and 300km, respectively